Nematic-driven anisotropic electronic properties of underdoped detwinned $Ba(Fe_{1-x}Co_x)_2As_2$ revealed by optical spectroscopy

C. Mirri,[1] A. Dusza,[1] S. Bastelberger,[1] J.-H. Chu,[2,3] H.-H. Kuo,[2,3] I. R. Fisher,[2,3] and L. Degiorgi[1]

[1]*Laboratorium für Festkörperphysik, ETH Zürich, CH-8093 Zürich, Switzerland*

[2]*Geballe Laboratory for Advanced Materials and Department of Applied Physics, Stanford University, Stanford, California 94305-4045, USA*

[3]*Stanford Institute for Materials and Energy Sciences, SLAC National Accelerator Laboratory, 2575 Sand Hill Road, Menlo Park, California 94025, USA*

(Received 25 August 2014; revised manuscript received 5 October 2014; published 21 October 2014)

We collect optical reflectivity data as a function of temperature across the structural tetragonal-to-orthorhombic phase transition at T_s on $Ba(Fe_{1-x}Co_x)_2As_2$ for $x = 0\%$, 2.5%, and 4.5%, with uniaxial and *in situ* tunable applied pressure in order to detwin the sample and to exert on it an external symmetry-breaking field. At $T < T_s$, we discover a remarkable hysteretic optical anisotropy as a function of the applied pressure at energies far away from the Fermi level. Such an anisotropy turns into a reversible linear pressure dependence at $T \geqslant T_s$. Moreover, the optical anisotropy gets progressively depleted with increasing Co content in the underdoped regime, consistent with the doping dependence of the orthorhombicity but contrary to the nonmonotonic behavior observed for the dc anisotropy.

DOI: 10.1103/PhysRevB.90.155125 PACS number(s): 74.70.Xa, 78.20.−e

The tetragonal-to-orthorhombic structural phase transition at T_s, coincident or preceding the onset of an antiferromagnetic ground state at T_N, in the underdoped regime of many families of iron-pnictide and chalcogenide superconductors breaks the fourfold rotational symmetry of the tetragonal phase, implying the onset of a nematic phase [1,2]. The relevance of nematicity, either electronic in nature or spin induced, in shaping their phase diagram is certainly one of the most debated issues nowadays [3–14]. Several experiments provide evidence for nematicity in iron pnictides, such as dc transport [15–20], thermopower [21], elastic shear modulus [22,23] also combined with nuclear magnetic resonance (NMR) results [24], neutron scattering [25–29], angle-resolved photoemission spectroscopy (ARPES) [30–32], local probes such as scanning tunneling microscopy (STM) [33–35] and magnetic torque [36], time-resolved spectroscopy [37,38], optical reflectivity [39–42], and Raman spectroscopy [43].

Detailed quantitative measurements of the in-plane charge and spin anisotropy in the nematic phase have been mainly performed on the so-called 122 family of iron pnictides, such as $Ba(Fe_{1-x}Co_x)_2As_2$, on which we focus here our attention. Since the ferroelastic-like structural transition induces in these materials the formation of dense structural twins below T_s in order to minimize the elastic energy, applying large magnetic fields [44] or uniaxial pressure turns out to be essential in order to detwin the specimens and thus to overrule the overcasting effect of randomly oriented domains when addressing the in-plane anisotropy of the orthorhombic phase over length scales greater than the average twin dimensions [1].

The vast majority of the experimental probes made use of applied uniaxial pressure in order to detwin the crystals. Besides the dc transport investigation with the piezo device [16], allowing tunable strain, experiments were performed with constantly applied pressure or possibly at low temperatures only. We were thus motivated to chase the fingerprint of the nematic phase into the charge dynamics, both as a function of temperature and applied pressure. For that purpose, we designed and constructed a pressure device [45], permitting us to tune moderate pressures (i.e., up to approximately 20 MPa) *in situ* and consequently giving us access to different experimental situations in terms of cooling procedures across T_s and T_N, and applied stress. The device (Fig. 1) consists of a spring bellows, which can be extended/retracted by flushing He gas into its volume or evacuating it through a capillary from outside the cryostat. This allows applying or releasing uniaxial pressure on the lateral side of the sample [46], thus modulating the strength of the external symmetry-breaking field and ultimately controlling the degree of detwinning.

A further goal of this paper is to expand our previous work, mainly devoted to the parent compound ($x = 0\%$) [45], to Co dopings spanning the underdoped regime of the $Ba(Fe_{1-x}Co_x)_2As_2$ phase diagram. For this study, single crystals of $Ba(Fe_{1-x}Co_x)_2As_2$ with $x = 0\%$, 2.5%, and 4.5% were grown using a self-flux method [15,16]. The structural (tetragonal-to-orthorhombic) and magnetic transitions, leading to antiferromagnetically ordered stripes, occur for $x = 0\%$ at $T_s \sim T_N \simeq 135$ K, for $x = 2.5\%$ at $T_s \simeq 98$ K and $T_N \simeq 92$ K whereas for $x = 4.5\%$ at $T_s \simeq 67$ K and $T_N \simeq 58$ K, respectively [1]. The last compound also undergoes a superconducting transition at $T_c \simeq 15$ K [1]. The as-grown single crystals have a platelike morphology with thickness between 0.1 and 0.3 mm and with the c axis perpendicular to the plane of the plates. They were cut into a square shape, approximately 2 mm on a side with the tetragonal a axis oriented at 45° to the edges of the sample so that upon cooling through T_s the orthorhombic a/b axes are parallel to the edges of the square and the orthorhombic shorter b axis is favored in the direction of the applied uniaxial compressive stress (Fig. 1) [1,15,16,45].

We performed optical investigations by measuring the reflectivity $R(\omega)$ at nearly normal incidence [47], first by collecting data at room temperature with different spectrometers: the Bruker IFS48 for the mid-infrared (MIR, 500–4000 cm^{-1}) and near-infrared (NIR, 4000–7000 cm^{-1}) frequency interval and the PerkinElmer Lambda 950 from NIR up to the ultraviolet (UV) range, i.e., 3200–48000 cm^{-1}.

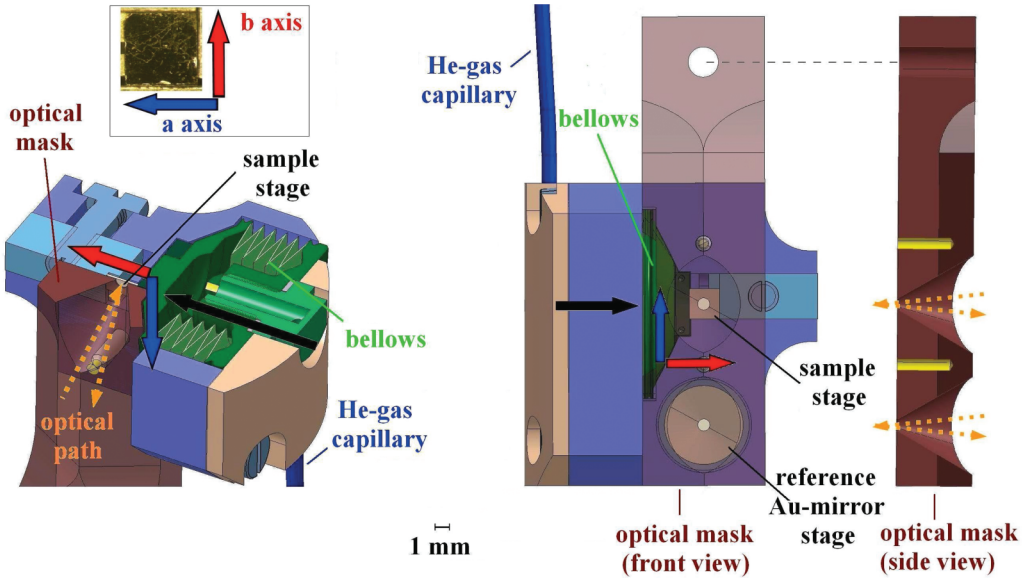

FIG. 1. (Color online) Left: Three-dimensional schematic view of the pressure device with a cross section along the plane of the incident/reflected optical path. Right: Front view along the light path [45]. By flushing He gas into the spring bellows and evacuating its volume, one can exert and release pressure, respectively, along the direction corresponding to the orthorhombic b axis, as indicated by the black arrow. The optical mask, placed on top of the pressure device, defines equal spots of the sample and reference Au-mirror surface, which are exposed to the electromagnetic radiation polarized along the a and b axes (blue and red arrows, respectively).

The specimens were then mounted into the pressure device (Fig. 1) and placed inside an Oxford SM 4000 cryostat coupled to a Fourier-transform infrared interferometer (Bruker Vertex 80v). This permits $R(\omega)$ measurements at different temperatures and as a function of pressure in the spectral range from the far-infrared (FIR) up to the NIR, i.e., between 30 and 6000 cm^{-1}. The electromagnetic radiation in all spectrometers was polarized along the a and b axes (Fig. 1); in the following the measured reflectivity will be defined as R_a and R_b, respectively [45]. In displaying the data, we refer to the He-gas pressure inside the volume of the pressure device (bellows). The effective pressure felt by the sample depends on its size and thickness, so that a He-gas pressure of 0.1 bars means an effective stress of about 1.5, 1.6, and 1.3 MPa for the $x = 0\%$, 2.5%, and 4.5% Co-doping samples, respectively. We refer to Ref. [45] and its supplemental information for more details on our experimental technique and setup. Here, we report results obtained from zero-pressure-cooled (ZPC) "pressure-loop" experiments: we reach the selected temperature (T) without applying pressure (p) and at that fixed T we measure $R(\omega)$ at progressively increasing p from 0 up to a maximum pressure ranging between 0.8 and 1.2 bars, depending on the Co doping. We subsequently collect $R(\omega)$ when stepwise releasing p back to 0 bars, thus completing the p loop. Additional experimental protocols that corroborate our findings are given in Ref. [45].

For the rest of the paper we focus our attention on the MIR spectral range, since clear signatures of the optical anisotropy have been previously recognized at those energies in experiments with samples constantly held under uniaxial stress [39–42]. Figure 2 displays a sampling of $R(\omega)$ data in the MIR range within the ZPC p-loop experiment at selected T for the $x = 2.5\%$ Co-doping compound. The results are very much representative for the underdoped regime and an equivalent set of data for the parent compound is available in the Supplemental Material of Ref. [45]. The emphasis in Figs. 2(a)–2(i) is at $T \ll T_s$, $T < T_s$, and $T \geqslant T_s$ and at $p = 0$ and 1.2 bars as well as at zero-released pressure. There is a crossover from a typical metallic behavior of $R(\omega)$ above T_s (i.e., monotonic increase towards total reflection for frequency tending to zero) to a depleted $R(\omega)$ at $T \ll T_s$, mainly due to the broad bump and flat $R(\omega)$ below about 1500 cm^{-1}. These latter features of $R(\omega)$ originate from the opening of a pseudogap-like excitation in the magnetic state [39–42]. While not shown, it is worth noting that even at $T < T_s$ $R(\omega)$ for both polarization directions tends to total reflection in a metallic-like fashion in the far-infrared spectral range (i.e., $\omega \leqslant 500$ cm^{-1}). In order to better highlight the evolution of the anisotropic charge dynamics as a function of the external tunable variables T and p, we calculate the reflectivity ratio $R_{\rm ratio}(\omega) = R_a(\omega)/R_b(\omega)$ [Figs. 2(l)–2(q)]. The anisotropy (polarization dependence) of $R(\omega)$ vanishes above 2500 cm^{-1} at all p (i.e., $R_{\rm ratio} \simeq 1$) but gets enhanced with decreasing T and increasing p at $\omega < 2500$ cm^{-1} and eventually saturates for $p \geqslant 0.8$ bars at $T < T_s$. At zero-released pressure, the optical anisotropy, before achieved at 1.2 bars, persists at $T \ll T_s$ [Figs. 2(l) and 2(o)] but is significantly reduced at $T < T_s$ [Figs. 2(m) and 2(p)]. At $T \geqslant T_s$, the p dependence of the optical anisotropy is fully reversible upon increasing and then decreasing p [Figs. 2(n) and 2(q)].

It is well established [48] that the real part $\sigma_1(\omega)$ of the optical conductivity displays a characteristic mid-infrared feature, peaked for twinned samples at frequencies (ω') between 900 cm^{-1} for $x = 4.5\%$ and 1500 cm^{-1} for $x = 0\%$ Co doping [vertical dotted lines in upper right panel (f) of Fig. 3]. Furthermore, this excitation turns out to be very much related to the onset of the SDW-like state in the orthorhombic phase

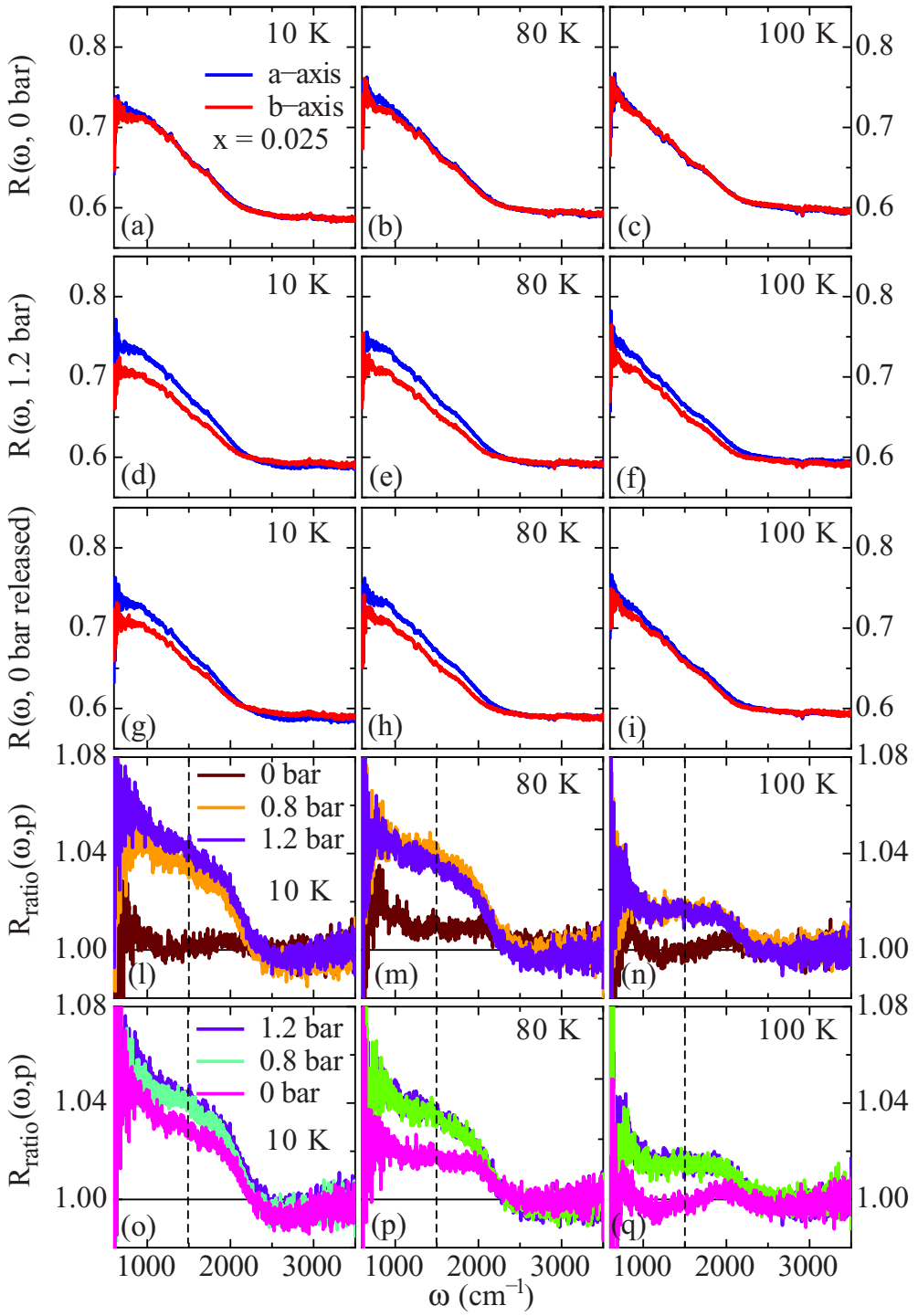

FIG. 2. (Color online) Temperature and pressure dependence of the optical reflectivity $R(\omega)$ for $Ba(Fe_{1-x}Co_x)_2As_2$ with $x = 2.5\%$ in the MIR spectral range at $T \ll T_s$, $T < T_s$, and $T \geqslant T_s$ and variable p [0 bars: (a)–(c), 1.2 bars: (d)–(f), zero-released pressure: (g)–(i)]. The blue and red curves in panels (a)–(i) refer to data collected with the electromagnetic radiation polarized along the a and b axis, respectively. $R_{\text{ratio}}(\omega, p) = R_a(\omega)/R_b(\omega)$ in panels (l)–(q) emphasizes the optical anisotropy [45], which is explicitly shown for increasing (0-0.8-1.2 bars) and decreasing (1.2-0.8-0 bars) pressures [(l)–(n) and (o)–(q), respectively]. The dashed vertical lines indicate the frequency where R_{ratio} is read (see text and Fig. 4 below).

and its polarization dependence was previously identified as the most evident signature of the pressure-induced optical anisotropy [39–42]. *Ab initio* calculations based on DFT as well as dynamical mean field theory (DMFT) [40,49–51] are rather powerful instruments in order to fairly reproduce the anisotropic MIR feature and to account for it as a fingerprint of the stripelike magnetic ordering in the orthorhombic state. This further supports our initial choice to mainly emphasize the MIR energy interval, pertinent to the electronic interband transitions. We can thus identify ω' as a relevant energy

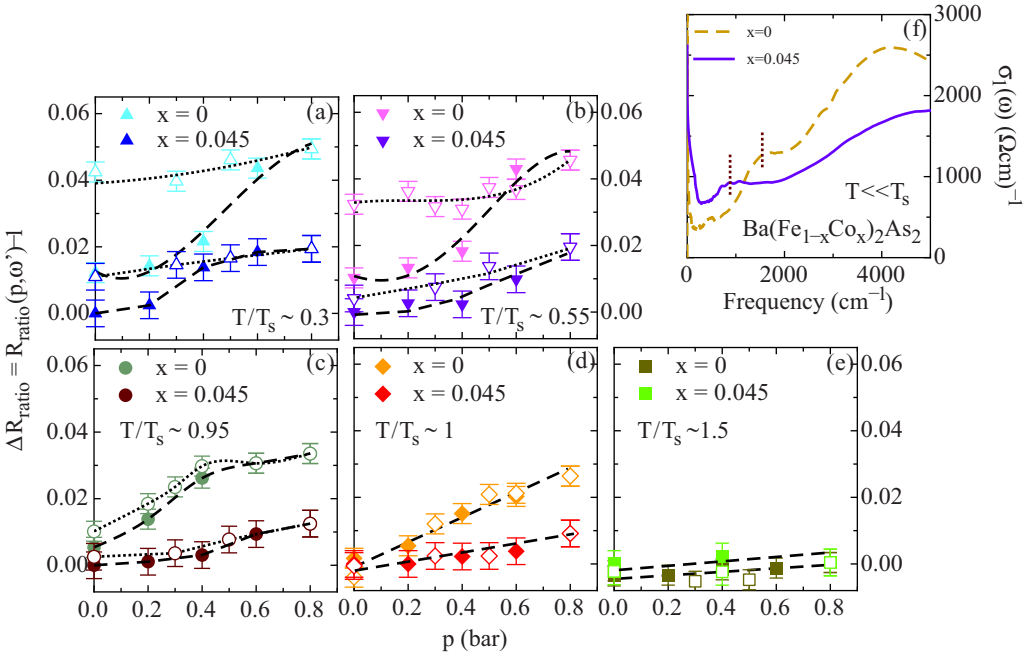

FIG. 3. (Color online) (a)–(e) Pressure dependence of $\Delta R_{\rm ratio} = R_{\rm ratio}(p,\omega') - 1$ at selected temperatures above and below T_s achieved in the ZPC "pressure-loop" experiment for $x = 0\%$ [45] and 4.5% Co doping (full and open symbols denote increasing and decreasing pressure, respectively). The dashed and dotted lines are guides for the eyes. The upper right panel (f) displays the real part $\sigma_1(\omega)$ of the optical conductivity for $x = 0\%$ and 4.5% Co doping at $T < T_s$, emphasizing the mid-infrared peak overlapped with the low-frequency tail of the stronger near-infrared absorption at about 4000 cm^{-1} (data from Ref. [48] on twinned specimens). The vertical dotted lines mark the position of the mid-infrared peak at $\omega' = 1500$ (1500) and 900 cm^{-1} for $x = 0\%$ (2.5%, not shown) and 4.5% Co doping, respectively, where $R_{\rm ratio}$ is read.

scale where to read $R_{\rm ratio}$. In order to comprehensively deploy our findings for the ZPC p-loop experiment, we show indeed in Figs. 3(a)–3(e) the pressure dependence for $x = 0\%$ and 4.5% Co doping of $\Delta R_{\rm ratio} = R_{\rm ratio} - 1$, defining the deviation from the isotropic case (i.e., $R_{\rm ratio} = 1$), at ω' and at temperatures above/below T_s. Figure 3 thus allows a comparison between two Co dopings of the title compounds, spanning the underdoped regime of their phase diagram. The pressure dependence of $\Delta R_{\rm ratio}$ for both compositions is rather similar at equivalent temperatures with respect to T_s, even though there is an overall depletion of $\Delta R_{\rm ratio}$ upon doping. We also remark that at $T \ll T_s$ $\Delta R_{\rm ratio}$ for the parent compound at $p = 0$ bars does not exactly vanish, suggesting a weak anisotropy (~1% or less), which is conceivably due to the partial detwinning caused by the thermal contraction of the pressure device and which however tends to be fully suppressed upon increasing temperature towards T_s and above it.

We first point out some common features for all Co dopings in $\Delta R_{\rm ratio}(p)$ at $T \ll T_s$. When increasing the applied pressure up to 0.2 bars there is yet a moderate increase of $\Delta R_{\rm ratio}$, which is then progressively enhanced for pressures around and exceeding 0.4 bars. The saturation in $\Delta R_{\rm ratio}$ for different Co dopings is observed to set in for applied pressures above 0.6 bars. The saturation presumably reflects when the samples are fully detwinned. In fact, it has been previously shown that pressures of about 1 bar (i.e., ~10 MPa as uniaxial pressure effectively felt by the sample) are enough in order to lead to a single domain specimen (see, e.g., Fig. 4 of Ref. [1]). Any subsequent pressure dependence, as shown in Fig. S6 of the Supplemental Material of Ref. [45], could arise from the intrinsic response to pressure of the orthorhombic structure [52]. Simultaneously, there is an overall decrease of the achieved optical anisotropy at saturation (see below, Fig. 4) for increasing Co doping. By releasing pressure back to zero and consequently by removing *in situ* the stress, the anisotropy clearly persists and hence a remarkable imbalance of the two twin orientations remains frozen in place at $T \ll T_s$. $\Delta R_{\rm ratio}$ at zero-released pressure could be then considered as a direct measurement of the optical anisotropy in a single domain specimen even in the absence of any applied stress. At $T \ll T_s$, there is thus a clear half-hysteresis behavior of $\Delta R_{\rm ratio}(p)$ [14], which is squeezed upon Co doping at equivalent T. Such a hysteretic behavior in detwinned iron-pnictides obviously bears a striking similarity with the situation in ferromagnets as far as the magnetization versus external magnetic field at $T \ll T_C$ (T_C being the Curie temperature) is concerned. In this context, we may coin the terms "initial anisotropy" or "virgin curve" and the term "remanent anisotropy" in order to define the evolution of $\Delta R_{\rm ratio}$, representing here the optical anisotropy, upon rising and releasing pressure, respectively. Finally, it is worth noting that the optical anisotropy, encountered at $T \ll T_s$, persists and remains unchanged even at $T < T_c$ for $x = 4.5\%$ Co doping. This would suggest that in the underdoped regime the electronic structure far away from the Fermi energy, as probed in the MIR-NIR spectral range, is unaffected by the onset of superconductivity.

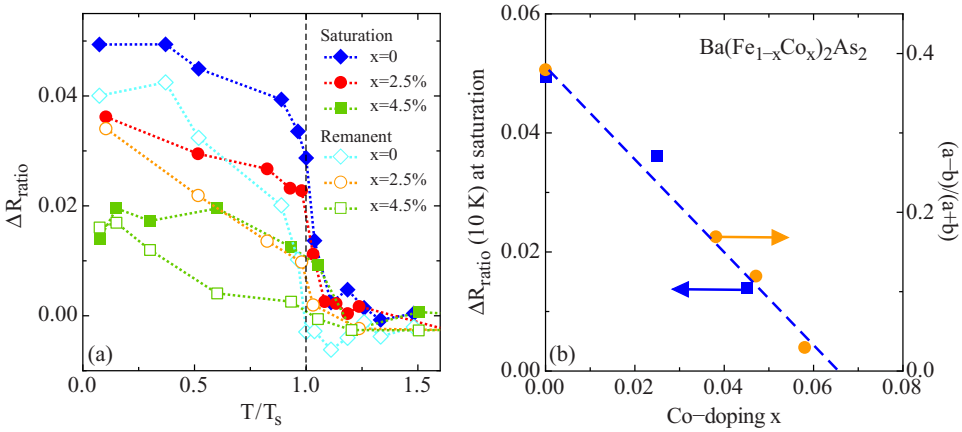

FIG. 4. (Color online) (a) Temperature dependence of $\Delta R_{\text{ratio}}(\omega')$ at saturation (i.e., at $p \geqslant 0.8$ bars, depending on Co doping) as well as at its remanent state (i.e., at released $p = 0$ bars) for $x = 0\%$ ($T_s \sim 135$ K), 2.5% ($T_s \sim 98$ K) [45], and 4.5% ($T_s \sim 67$ K) Co doping. The T axis is normalized by T_s and ω' is defined by the vertical dotted lines in Fig. 3(f). (b) Co doping dependence (x) of ΔR_{ratio} at 10 K and at saturation [from panel (a)] and of the orthorhombicity $(a - b)/(a + b)$ [53].

By increasing T towards T_s, we observe, commonly to all Co dopings, a narrowing of the hysteretic behavior, which fully collapses at $T \sim T_s$. Moreover, at zero-released pressure ΔR_{ratio} is substantially reduced upon increasing T, since the thermally assisted domain-wall motion leads to retwinning of the sample in a stress-free environment [45]. Above T_s there should not be any hysteresis since the material is tetragonal, as indeed observed experimentally. At $T \geqslant T_s$, the pressure dependence of ΔR_{ratio} may well be approximated with a linear behavior. These observations further reinforce the notion that there seems to be an equivalent impact of the pressure on ΔR_{ratio} in the title compounds as of the magnetic field with respect to the magnetization in a ferromagnet. In summary, we may state that the hysteretic behavior, observed in ΔR_{ratio} below T_s, arises due to the blocking of the twin boundary motion [14], which then appears to be thermally activated upon increasing T.

We shall now try to place our optical findings for all investigated Co-doped 122 iron pnictides into a common context and perspective. Figure 4(a) displays the temperature dependence of ΔR_{ratio} for $x = 0\%$, 2.5%, and 4.5% Co doping at pressures where saturation occurs in the optical anisotropy (i.e., $p \geqslant 0.8$ bars at $T < T_s$, depending from the doping) as well as at released $p = 0$ bars (i.e., so-called remanent state), with the T scale normalized by T_s of each composition. There is a similar behavior for all compounds. First of all, the temperature dependence of ΔR_{ratio} at the remanent state undergoes a sudden drop close to and above T_s, which further points out the effect of the thermal activation of the twin boundary motion. Second, the inspection of the data reported in Figs. 3(a)–3(e) and 4(a) emphasizes that the largest optical anisotropy at saturation and at $T < T_s$ is achieved for $x = 0\%$. While several factors may influence the doping dependence, the largest anisotropy for $x = 0\%$ rather than for $x = 2.5\%$ or $x = 4.5\%$ Co doping could derive from a stronger order parameter of the structural phase transition in the parent compound. Alternatively, we may state that the depleted optical anisotropy upon doping, at saturation and at each $T < T_s$, implies a decreasing lattice softness, going hand in hand with the Co-content dependence of the orthorhombicity $(a - b)/(a + b)$ (a and b are the lattice constants of the respective axes) [12]. This is explicitly shown in Fig. 4(b), which compares the Co-doping dependence (x) of ΔR_{ratio} at saturation for $T \ll T_s$ with respect to the measured orthorhombicity in $Ba(Fe_{1-x}Co_x)_2As_2$ [53]. Such a direct relationship between ΔR_{ratio} at saturation and $(a - b)/(a + b)$ contrasts with the nonmonotonic anisotropy of the dc transport data upon doping [1,15]. This might be the consequence of the multiband nature of the title compounds. Since transport measurements are only sensitive to small energy scales close to the Fermi level, it is possible to get quite nonmonotonic behavior of the transport anisotropy across the phase diagram depending on what the underlying bands are doing. Moreover, the nonmonotonic resistivity anisotropy mainly appears in the antiferromagnetic state, where the Fermi surface (FS) has been severely reconstructed and Lifshitz transitions may occur as a function of doping. It was suggested that the small in-plane dc anisotropy in the parent compound is mainly the consequence of the presence of an isotropic high-mobility Dirac pocket, which is progressively suppressed upon doping [54]. In this sense, the resistivity anisotropy certainly does not have to track better avatars of the nematic order parameter as a function of doping and can be only revealed when the contribution due to the remaining anisotropic FS pockets dominates upon chemical substitution. Therefore, the comparison proposed in Fig. 4(b) may indicate that a direct mapping of the orthorhombicity and consequently of nematicity into the electronic structure can be identified most clearly at energy scales away from the Fermi level.

Furthermore, ΔR_{ratio} at saturation is temperature dependent already above T_s, with a broad crossover through the structural transition [Fig. 4(a)] [55]. Such a pressure-induced orthorhombicity in the paramagnetic state provides some evidence for a substantial susceptibility, as a fingerprint of the fluctuations related to the nematic-driven ferroelastic structural transition. In this context, we recall the linear p dependence of ΔR_{ratio} for $T \geqslant T_s$ [Figs. 3(d) and 3(e)]. In our previous work [45], we have proposed to calculate its slope $(\Delta R_{\text{ratio}}/p)$ as a function of temperature, which was claimed to represent an (optical)

estimation of the nematic susceptibility, very similar to the outcome from the dc data [16].

Our findings about the pressure-induced optical anisotropy, common to the whole underdoped regime, are in broad agreement with ARPES data [30,31] on detwinned specimens. ARPES results are very instrumental in revealing an in-plane electronic anisotropy characterized by a large energy splitting of two orthogonal bands with dominant d_{xz} and d_{yz} character. Such a band splitting already develops at $T > T_s$ for stressed crystals and may indicate a pressure-induced orbital ordering. This naturally accounts for our findings on the optical anisotropy in terms of dichroism, generated by the external symmetry-breaking field [4]. Upon doping, the onset of the band splitting, observed in ARPES [30,31], is bound to the structural phase transition, in agreement with the optical data displayed in Figs. 3(a)–3(e). The band splitting extends much less above T_s for unstressed than for stressed crystals, which backs up our analysis of $\Delta R_{\rm ratio}$ at saturation and for the remanent state deployed in Fig. 4(a). As anticipated above and as well established by dc transport [16] and by NMR and elastic shear moduli experiments [22–24], the ferropnictides suffer an anomalously large nematic susceptibility, explaining the large electronic anisotropy observed for strained samples in ARPES [30,31] and inferred by the current optical work at $T > T_s$.

On the contrary, even though our measurements for underdoped specimens certainly point out an extensive fluctuation regime above T_N, within which the ferroelastic transition at T_s occurs, there is no need, based on our data, to invoke the onset of the nematic phase transition at $T^* > T_s$, as proposed for instance by the magnetotorque experiment [36].

In conclusion, we demonstrate the capability of optics to get insights into the nematic-driven tetragonal-to-orthorhombic structural transition in the underdoped regime of the title compounds. The main findings evinced from our work are (i) the capability to release *in situ* p, as symmetry breaking field, and thus to observe the anisotropy of the electrodynamic response at $T \ll T_s$ for unstressed but fully detwinned crystals, and (ii) the hysteretic nature of the optical anisotropy upon varying the stress due to the motion of the nematic domain walls. Our data give clear-cut evidence for the impact of the ferroelastic transition at energy scales deep into the electronic structure and for its fluctuations over a remarkable temperature interval above T_s. The discovered optical fingerprint of the nematic fluctuations originates from an intrinsic pressure-induced electronic anisotropy and bears testimony to the electronic nature of the structural phase transition. We have not observed any changes in the optical anisotropy at $T < T_c$ in the underdoped regime, which would suggest that superconductivity emerges within an electronic polarized state. Our results could equally favor scenarios for the structural and magnetic transitions in the underdoped regime based on the ferro-orbital ordering [3–8], which implies the involvement of spin-orbital coupling, or any models related to a spin-driven nematic order affecting however the charge channel of the excitation spectrum [9–13]. In conjunction with other studies [16,19,27,30,31,43] we nonetheless speculate that the orbital degree of freedom as well as its precursor effects above T_s are indispensable ingredients at least in characterizing the normal-state properties out of which superconductivity develops in the iron pnictides.

As for the future, this work paves the way for a systematic survey of the generic phase diagram, going beyond the underdoped regime, and specifically of the far-infrared optical properties. These latter experiments, presently in progress, will permit the analysis of the effective metallic contribution in the charge dynamics in terms of Drude weight and scattering rates of the itinerant charge carriers, thus allowing a more robust link to the dc transport properties. Furthermore, it could be of interest to compare our results achieved on electron-doped materials with data collected on hole-doped ones, and to possibly use the hysteretic behavior in order to precisely test the impact of doping-induced disorder [14], thus expanding at finite frequencies the debate already addressed by dc transport investigations [42,56,57].

The authors wish to thank A. Lucarelli for his initial contribution in designing the pressure device and E. Bascones, W. Ku, E. W. Carlson, M. Sigrist, S. Kivelson, T. Devereaux, and D. Lu for fruitful discussions. Work at ETH Zurich was supported by the Swiss National Science Foundation and Work at Stanford University was supported by the DOE, Office of Basic Energy Sciences, under Contract No. DE-AC02-76SF00515.

[1] I. R. Fisher, L. Degiorgi, and Z. X. Shen, Rep. Prog. Phys. **74**, 124506 (2011) and references therein.
[2] M. A. Tanatar, A. Kreyssig, S. Nandi, N. Ni, S. L. Bud'ko, P. C. Canfield, A. I. Goldman, and R. Prozorov, Phys. Rev. B **79**, 180508(R) (2009).
[3] C.-C. Lee, W.-G. Yin, and W. Ku, Phys. Rev. Lett. **103**, 267001 (2009).
[4] C.-C. Chen, J. Maciejko, A. P. Sorini, B. Moritz, R. R. P. Singh, and T. P. Devereaux, Phys. Rev. B **82**, 100504(R) (2010).
[5] W. Lv, F. Krüger, and P. Phillips, Phys. Rev. B **82**, 045125 (2010).
[6] W. Lv and P. Phillips, Phys. Rev. B **84**, 174512 (2011).
[7] X. Zhang and E. Dagotto, Phys. Rev. B **84**, 132505 (2011).
[8] Z. Wang and A. H. Nevidomskyy, arXiv:1408.1408.
[9] R. M. Fernandes and A. J. Millis, Phys. Rev. Lett. **111**, 127001 (2013).
[10] C. Fang, H. Yao, W.-F. Tsai, J. P. Hu, and S. A. Kivelson, Phys. Rev. B **77**, 224509 (2008).
[11] C. Xu, M. Müller, and S. Sachdev, Phys. Rev. B **78**, 020501(R) (2008).
[12] R. M. Fernandes, A. V. Chubukov, J. Knolle, I. Eremin, and J. Schmalian, Phys. Rev. B **85**, 024534 (2012); **85**, 109901(E) (2012).
[13] R. M. Fernandes, A. V. Chubukov, and J. Schmalian, Nat. Phys. **10**, 97 (2014).
[14] E. W. Carlson and K. A. Dahmen, Nat. Commun. **2**, 379 (2011).
[15] J.-H. Chu, J. G. Analytis, K. De Greve, P. L. McMahon, Z. Islam, Y. Yamamoto, and I. R. Fisher, Science **329**, 824 (2010).
[16] J.-H. Chu, H.-H. Kuo, J. G. Analytis, and I. R. Fisher, Science **337**, 710 (2012).
[17] A. F. Wang, J. J. Ying, X. G. Luo, Y. J. Yan, D. Y. Liu, Z. J. Xiang, P. Cheng, G. J. Ye, L. J. Zou, Z. Sun, and X. H. Chen, New J. Phys. **15**, 043048 (2013).

[18] J. J. Ying, X. F. Wang, T. Wu, Z. J. Xiang, R. H. Liu, Y. J. Yan, A. F. Wang, M. Zhang, G. J. Ye, P. Cheng, J. P. Hu, and X. H. Chen, Phys. Rev. Lett. **107**, 067001 (2011).

[19] E. C. Blomberg, M. A. Tanatar, R. M. Fernandes, I. I. Mazin, B. Shen, H.-H. Wen, M. D. Johannes, J. Schmalian, and R. Prozorov, Nat. Commun. **4**, 1914 (2013).

[20] H.-H. Kuo, M. C. Shapiro, S. C. Riggs, and I. R. Fisher, Phys. Rev. B **88**, 085113 (2013).

[21] S. Jiang, H. S. Jeevan, J. Dong, and P. Gegenwart, Phys. Rev. Lett. **110**, 067001 (2013).

[22] R. M. Fernandes, L. H. VanBebber, S. Bhattacharya, P. Chandra, V. Keppens, D. Mandrus, M. A. McGuire, B. C. Sales, A. S. Sefat, and J. Schmalian, Phys. Rev. Lett. **105**, 157003 (2010).

[23] A. E. Böhmer, P. Burger, F. Hardy, T. Wolf, P. Schweiss, R. Fromknecht, M. Reinecker, W. Schranz, and C. Meingast, Phys. Rev. Lett. **112**, 047001 (2014).

[24] R. M. Fernandes, A. E. Böhmer, C. Meingast, and J. Schmalian, Phys. Rev. Lett. **111**, 137001 (2013).

[25] C. Dhital, Z. Yamani, W. Tian, J. Zeretsky, A. S. Sefat, Z. Wang, R. J. Birgeneau, and S. D. Wilson, Phys. Rev. Lett. **108**, 087001 (2012).

[26] L. W. Harriger, H. Q. Luo, M. S. Liu, C. Frost, J. P. Hu, M. R. Norman, and P. Dai, Phys. Rev. B **84**, 054544 (2011).

[27] Y. Song, S. V. Carr, X. Lu, C. Zhang, Z. C. Sims, N. F. Luttrell, S. Chi, Y. Zhao, J. W. Lynn, and P. Dai, Phys. Rev. B **87**, 184511 (2013).

[28] S. Avci, O. Chmaissem, J. M. Allred, S. Rosenkranz, I. Eremin, A. V. Chubukov, D. E. Bugaris, D.-Y. Chung, M. G. Kanatzidis, J.-P. Castellan, J. A. Schlueter, H. Claus, D. D. Khalyavin, P. Manuel, A. Daoud-Aladine, and R. Osborn, Nat. Commun. **5**, 3845 (2014).

[29] X. Lu, J. T. Park, R. Zhang, H. Luo, A. H. Nevidomskyy, Q. Si, and P. Dai, Science **345**, 657 (2014).

[30] M. Yi, D. Lu, J.-H. Chu, J. G. Analytis, A. P. Sorini, A. F. Kemper, B. Moritz, S.-K. Mo, R. G. Moore, M. Hashimoto, W.-S. Lee, Z. Hussain, T. P. Devereaux, I. R. Fisher, and Z.-X. Shen, Proc. Natl. Acad. Sci. USA **108**, 6878 (2011).

[31] M. Yi, D. H. Lu, R. G. Moore, K. Kihou, C.-H. Lee, A. Iyo, H. Eisaki, T. Yoshida, A. Fujimori, and Z.-X. Shen, New J. Phys. **14**, 073019 (2012).

[32] Q. Wang, Z. Sun, E. Rotenberg, F. Ronning, E. D. Bauer, H. Lin, R. S. Markiewicz, M. Lindroos, B. Barbiellini, A. Bansil, and D. S. Dessau, Phys. Rev. B **88**, 235125 (2013).

[33] T.-M. Chuang, M. P. Allan, J. Lee, Y. Xie, N. Ni, S. L. Bud'ko, G. S. Boebinger, P. C. Canfield, and J. C. Davis, Science **327**, 181 (2010).

[34] M. P. Allan, T.-M. Chuang, F. Massee, Y. Xie, N. Ni, S. L. Bud'ko, G. S. Boebinger, Q. Wang, D. S. Dessau, P. C. Canfield, M. S. Golden, and J. C. Davis, Nat. Phys. **9**, 220 (2013).

[35] E. P. Rosenthal, E. F. Andrade, C. J. Arguello, R. M. Fernandes, L. Y. Xing, X. C. Wang, C. Q. Jin, A. J. Millis, and A. N. Pasupathy, Nat. Phys. **10**, 225 (2014).

[36] S. Kasahara, H. J. Shi, K. Hashimoto, S. Tonegawa, Y. Mizukami, T. Shibauchi, K. Sugimoto, T. Fukuda, T. Terashima, A. H. Nevidomskyy, and Y. Matsuda, Nature (London) **486**, 382 (2012).

[37] L. Stojchevska, T. Mertelj, J.-H. Chu, I. R. Fisher, and D. Mihailovic, Phys. Rev. B **86**, 024519 (2012).

[38] A. Patz, T. Li, S. Ran, R. M. Fernandes, J. Schmalian, S. L. Bud'ko, P. C. Canfield, I. E. Perakis, and J. Wang, Nat. Commun. **5**, 3229 (2014).

[39] A. Dusza, A. Lucarelli, F. Pfuner, J.-H. Chu, I. R. Fisher, and L. Degiorgi, Europhys. Lett. **93**, 37002 (2011).

[40] A. Dusza, A. Lucarelli, A. Sanna, S. Massidda, J.-H. Chu, I. R. Fisher, and L. Degiorgi, New J. Phys. **14**, 023020 (2012).

[41] M. Nakajima, T. Liang, S. Ishida, Y. Tomioka, K. Kihou, C. H. Lee, A. Iyo, H. Eisaki, T. Kakeshita, T. Ito, and S. Uchida, Proc. Natl. Acad. Sci. USA **108**, 12238 (2011).

[42] M. Nakajima, S. Ishida, Y. Tomioka, K. Kihou, C. H. Lee, A. Iyo, T. Ito, T. Kakeshita, H. Eisaki, and S. Uchida, Phys. Rev. Lett. **109**, 217003 (2012).

[43] Y. Gallais, R. M. Fernandes, I. Paul, L. Chauvière, Y.-X. Yang, M.-A. Méasson, M. Cazayous, A. Sacuto, D. Colson, and A. Forget, Phys. Rev. Lett. **111**, 267001 (2013).

[44] J. P. C. Ruff, J.-H. Chu, H.-H. Kuo, R. K. Das, H. Nojiri, I. R. Fisher, and Z. Islam, Phys. Rev. Lett. **109**, 027004 (2012).

[45] C. Mirri, A. Dusza, S. Bastelberger, J.-H. Chu, H.-H. Kuo, I. R. Fisher, and L. Degiorgi, Phys. Rev. B **89**, 060501(R) (2014), and Supplemental Material therein.

[46] The pressure device (Fig. 1) [45] is superior to the piezo technique [16]. The latter performs well at high temperatures, allowing a realistic investigation of the nematic susceptibility (at $T \geqslant T_s$), but less so at low temperatures due to the limited dynamic range of the piezo itself.

[47] M. Dressel and G. Grüner, *Electrodynamics of Solids* (Cambridge University Press, Cambridge, England, 2002).

[48] A. Lucarelli, A. Dusza, F. Pfuner, P. Lerch, J. G. Analytis, J.-H. Chu, I. R. Fisher, and L. Degiorgi, New J. Phys. **12**, 073036 (2010).

[49] A. Sanna, F. Bernardini, G. Profeta, S. Sharma, J. K. Dewhurst, A. Lucarelli, L. Degiorgi, E. K. U. Gross, and S. Massidda, Phys. Rev. B **83**, 054502 (2011).

[50] Z. P. Yin, K. Haule, and G. Kotliar, Nat. Phys. **7**, 294 (2011).

[51] K. Sugimoto, E. Kaneshita, and T. Tohyama, J. Phys. Soc. Jpn. **80**, 033706 (2011).

[52] At $T \ll T_s$, the optical anisotropy for all Co dopings tends to saturate for applied pressures of He gas between 0.8 and 1 bar [Figs. 3(a)–3(e)]; i.e., approximately 15 MPa as pressure effectively felt by the sample, which corresponds to pressure values of about a factor 10 smaller than predicted by M. Tomić, H. O. Jeschke, R. M. Fernandes, and R. Valentí, Phys. Rev. B **87**, 174503 (2013).

[53] R. Prozorov, M. A. Tanatar, N. Ni, A. Kreyssig, S. Nandi, S. L. Bud'ko, A. I. Goldman, and P. C. Canfield, Phys. Rev. B **80**, 174517 (2009).

[54] H.-H. Kuo, J.-H. Chu, S. C. Riggs, L. Yu, P. L. McMahon, K. De Greve, Y. Yamamoto, J. G. Analytis, and I. R. Fisher, Phys. Rev. B **84**, 054540 (2011).

[55] The broadening of ΔR_{ratio} was found to get enhanced the larger the applied pressure is (see Fig. 4 in Ref. [45]), so that its temperature dependence at saturation (i.e., $p \geqslant 0.8$ bars, depending on the Co doping) looks quite similar to the behavior of the dc anisotropy for temperatures above T_s in equivalent experimental conditions [15,45].

[56] S. Ishida, M. Nakajima, T. Liang, K. Kihou, C. H. Lee, A. Iyo, H. Eisaki, T. Kakeshita, Y. Tomioka, T. Ito, and S. Uchida, Phys. Rev. Lett. **110**, 207001 (2013).

[57] H.-H. Kuo and I. R. Fisher, Phys. Rev. Lett. **112**, 227001 (2014).